LASER & PHOTONICS REVIEWS
www.lpr-journal.org

Soft Mesocrystal Enabled Multi-Degree Light Modulation

Quanming Chen, Xinyue Wang, Chunting Xu, Hongchen Chu, Hongguan Yu, Cheng Ouyang, Yun Lai, Zhigang Zheng, Xiao Liang, Yanqing Lu, and Wei Hu**

Mesocrystals introduce high-level orders, such as chirality, topology, and hierarchy to the crystallography, and thus bring collective and emergent properties beyond traditional crystals. Orthogonally modulating the multiple degrees of light is highly pursued to fully explore the intrinsic multidimensional and large-scale parallel processing capability of photon informatics. Unfortunately, it is unachievable with traditional light–matter interaction systems. Here, the multi-degree light modulation is realized based on the hierarchical architecture of a soft mesocrystal. High-quality monodomains of both blue phase I and blue phase II are formed via regulating the assembly of liquid crystals by photoalignment anchoring and electricity. The mapping relationship between optical freedoms (the spin, wavelength, and geometric phase of light) and hierarchical structures (the chirality of helix, lattice constant, and the azimuthal orientation of cubic lattices) is established. Omnidirectional spatial phase modulation with spin and full color selectivity is demonstrated. Based on the multi-degree light modulation, 3D and wavelength-selective orbital angular momentum generation as well as multichannel color holographic display are presented. This work extends the fundamental understanding of blue phase mesocrystals and provides a promising strategy for large-scale parallel and multi-degree light modulation that may be utilized in vital fields, such as supercomputing, optical communications, and virtual/augmented realities.

1. Introduction

The mesocrystal composed of aligned nanosized crystals depicts a heterogeneously ordered structure distinguished from classical single crystals and polycrystals.[1] Repeatable units of diverse species and geometries assemble into mesocrystals via physical interactions and spatial constraints, thus introducing fascinating symmetry breakings, such as chirality, topology, and hierarchy.[2] Such superstructures bring collective and emergent properties beyond traditional crystals formed by periodic atoms, ions, or molecules. Mesocrystals are evolutionarily favored in biominerals, which significantly improve the mechanical performance of creatures, such as sea urchin spines.[3] This inspires a biomimetic strategy for synthesizing artificial materials with upgraded features. In addition to the unusual mechanical properties, the hierarchically ordered structures drastically enhance the charge capacity of sodium-ion batteries[4] as well as the efficiency of photoelectrochemical H_2O_2 production.[5] Narrow band terahertz emission originates from the propagation of coherent vibration among mesocrystal microspheres.[6] Despite these impressive progresses, the weak driving force as well as the diversity of units lead to the formation of mesocrystals fragile and make the underlying dynamics and mechanisms elusive.[7] Therefore, it is challenging to construct hierarchical structures precisely in a predictable manner. Moreover, dynamic manipulations and extra hierarchies are expected to be further introduced to mesocrystals for the sake of more fantastic characteristics. Exploiting uncharted territories that can make full use of the hierarchy of mesocrystals is also an urgent task.

Currently, vital fields, such as supercomputing, optical communications, and virtual/augmented realities desire superlarge-capacity information processing. Photon informatics exhibits superiority to electronic techniques due to its intrinsic multidimensional and large-scale parallel processing. Thus, accurately, efficiently, and orthogonally manipulating the multiple degrees of freedom of light is highly pursued. Unfortunately, it is unachievable with traditional light–matter interaction systems. Recently, free manipulations of the amplitude, phase, polarization, and wavelength of light have been achieved using an

Q. Chen, X. Wang, C. Xu, H. Yu, C. Ouyang, Y. Lu, W. Hu
National Laboratory of Solid State Microstructures
College of Engineering and Applied Sciences
Nanjing University
Nanjing 210023, China
E-mail: yqlu@nju.edu.cn; huwei@nju.edu.cn
H. Chu, Y. Lai
National Laboratory of Solid State Microstructures
School of Physics
and Collaborative Innovation Center of Advanced Microstructures
Nanjing University
Nanjing 210093, China
Z. Zheng
Department of Physics
East China University of Science and Technology
Shanghai 200237, China
X. Liang
Department of Chemistry
Tsinghua University
Beijing 100084, China

The ORCID identification number(s) for the author(s) of this article can be found under https://doi.org/10.1002/lpor.202301283

DOI: 10.1002/lpor.202301283

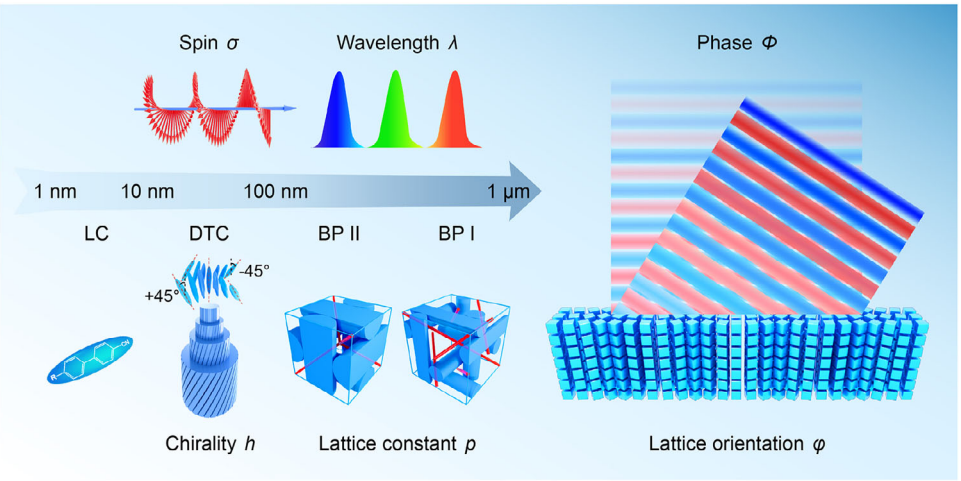

Figure 1. Schematic illustration of hierarchical BPLC mesocrystal-enabled multi-degree light modulation.

ultrathin metasurface by tailoring the geometry and spatial distribution of subwavelength resonators.[8] However, such devices suffer from costly and sophisticated top-down fabrication and limited multiplexing capability for static functions. Therefore, affordable bottom-up technologies for flexible multi-degree light modulation are highly sought after. Liquid crystal (LC) is a typical electro-optical material widely utilized in information display and telecom industries.[9] It also functions as a building block that forms various phases and textures.[10] Blue phase LCs (BPLCs) consist of cubic lattices assembled by LC double twisted cylinders (DTCs).[11] Due to the crystallographically hierarchical structure and sensitivity to external fields, the BPLC can be regarded as a soft mesocrystal. However, the randomly oriented lattices degrade the Bragg reflection and cause serious scattering.[12] To realize a large-area monodomain, various physical fields have been adopted to suppress random nucleation. Unidirectional surface anchoring[13] and patterned hybrid alignments[14] are proven to effectively homogenize lattice orientations by supplying uniform nucleation sites. Long lasting electric[15] and acoustic[16] fields promote the generation of monodomain by aligning the LC molecules for assembly. Additionally, gradient temperature scanning directs the preferential growth direction of the mesocrystal to enlarge the domain size.[17] Recently, geometric phase modulations are implemented by presetting the azimuthal orientation of BP lattices.[18] However, the assembly dynamics is still unclear, hindering the high-quality fabrication of deliciated BP mesocrystals. Moreover, the structure–activity relationship between the configurations of hierarchies and parameters of light is ambiguous, and individual tuning of hierarchies has not yet been achieved, both of which are highly desirable for mesocrystal-based multi-degree light modulations.

We adopt photoalignment to realize high-quality BP mesocrystals and further introduce a vertical electric field to keep the hierarchy undestroyed during the phase transition. By this means, centimeter-size monodomains are obtained in all BP phases, enabling a sharp and full color selective reflection. The one-to-one correspondences between the chirality of DTC, the cubic lattice constant, the azimuthal orientation of the cubic lattice and the spin angular momentum (SAM) of light, wavelength, and geometric phase have been theoretically established and experimentally verified. By presetting the in-plane distribution of cubic lattices, omnidirectionally spin-orbital coupling of light is realized with high efficiency. Orbital angular momentum (OAM) generation and reconfigurable holographic displays are demonstrated by properly programming the hierarchical structures of the BP mesocrystals. This work paves a way for high-quality soft mesocrystal assembly and provides a promising strategy for large-scale parallel and multi-degree light modulation.

2. Results

2.1. Hierarchical BPLC Mesocrystal Enabled Multi-Degree Light Modulation

Figure 1 vividly illustrates the hierarchical structure of BPLCs. When mixed with chiral dopants to induce strong twisting power, the elongated single-nanometer-sized LC molecules double twist to form cylinders of tens of nanometers in diameter, i.e., DTCs. In each DTC, the director is parallel to the cylinder axis at the center and rotates ±45° continuously around the opposite radii (only two pairs of them are exhibited in Figure 1). Such DTCs further assemble into cubic structures and form BP lattices (hundreds of nanometers in size), which possess simple cubic for the BP II phase and body-centered cubic for the BP I phase. The DTCs cannot tile the whole 3D space, leading to inevitable disclinations (redlines in the lattices). The exotic arrangement characteristic endows the BPLC with an omnidirectional spin-selective Bragg reflection. The chirality (h) of DTCs determines the spin (σ, circular polarization) of the reflected light, while the central wavelength (λ) is governed by the lattice constants (p). If one can locally tailor the azimuthal orientation (φ) of BP lattices, the Pancharatnam–Berry (PB) phase (Φ), which originates from the polarization evolution of the reflected light, can be modulated with a phase difference equal to half of the solid angle encompassed by the closed trajectory on the Poincare sphere.[19] Because the freedoms $\{h, p, \varphi\}$ of hierarchical structures can be

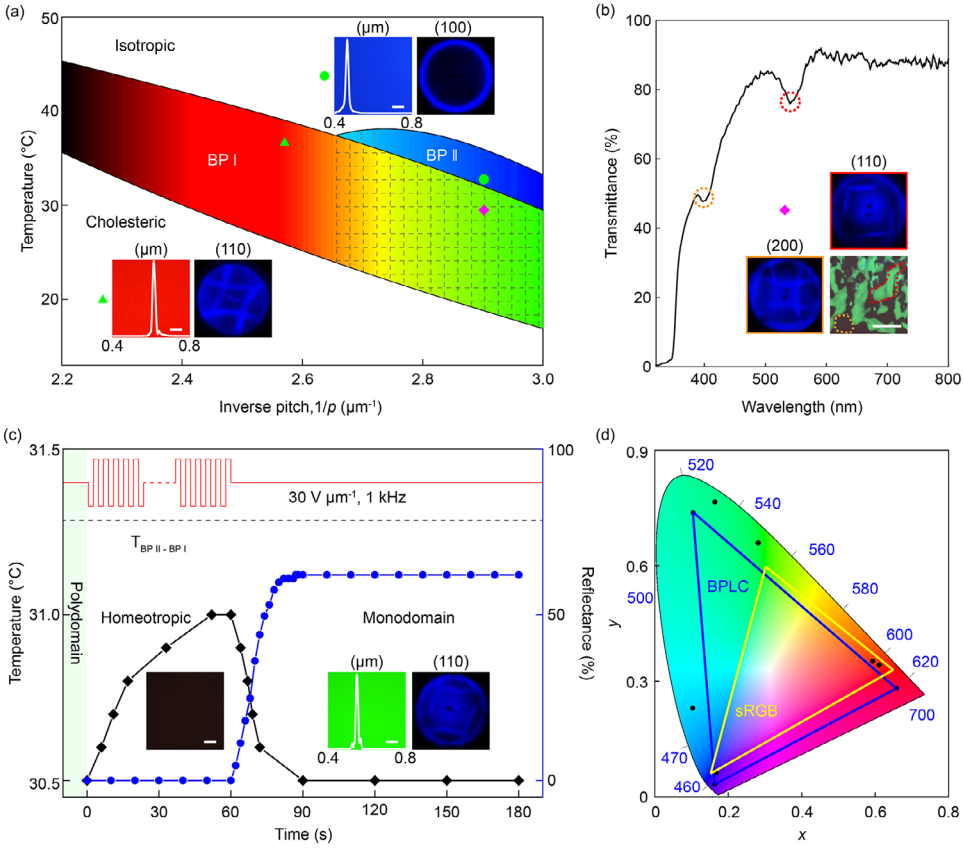

Figure 2. Growth of the BPLC monodomain. a) The phase diagram of a unidirectionally photoaligned BPLC. Insets show the POM images with reflection spectra and Kossel diagrams of BP II (green disk) and BP I (green triangle), respectively. The filled color indicates the corresponding reflection band. b) The transmission spectrum of the BP I polydomain transformed from the BP II monodomain as denoted by the purple diamond in (a). Insets show the POM image and Kossel diagrams recorded at red and orange dashed lines marked regions. c) Dependencies of temperature and reflectance on the applied electric field (red line). The black dashed line indicates the phase transition temperature between BP II and BP I. Insets show the POM image of the homeotropic state, the POM image with the reflection spectrum and the Kossel diagram of the BP I monodomain converted from BP I multidomain. d) Chromatic coordinates of different BPLC reflection bands compared with the sRGB in the CIE 1931 diagram. All scale bars indicate 200 μm.

independently and precisely preset, multiple degrees $\{\sigma, \lambda, \Phi\}$ of light are thus expected to be orthogonally modulated. However, it is challenging to realize an ideal hierarchical architecture and precisely tailor its structural freedoms because entropy-driven self-assembly usually generates polydomains, breaks the continuity of the mesocrystal and thus restricts its optical and photonic applications. Therefore, it is highly necessary to explore state-of-the-art techniques to construct desirable mesocrystals and fully release their potential.

2.2. External-Field Driven Growth of the BPLC Monodomain

Unidirectional and noncontact photoalignment uniformly guides the lattice orientation and thus facilitates the generation of a large-area BP monodomain. **Figure 2a** shows the phase diagram dependent on the chiral strength $1/p$, $p = c$*HTP, where c and HTP are the weight concentration and helical twisting power of the chiral dopant, respectively. When cooling from the isotropic state directly to the BP I phase and BP II phase at a rate of −0.3 °C min^{-1}, the uniform textures with saturated reflective colors under a polarizing optical microscope (POM) and sharp reflection spectra reveal the high-quality factor of the generated BPLC mesocrystals. The Kossel diagrams (Figure S1, Supporting Information) suggest that the crystallographic planes normal to the observation are (110) for BP I and (100) for BP II. Notably, BP II favors strong chirality; therefore, a monodomain is not achievable when $1/p$ is just over the triple point. Moreover, LC molecules reorient significantly to arrange the new hierarchical structure during the BP II-BP I phase transition. Sole alignment cannot support the growth of the BP I monodomain. The multidomain of BP I, widely observed in previous studies as well,[14b,20] is obtained (grid lines denote the region in Figure 2a). Two valleys with minima at 540 and 397 nm are separately observed in Figure 2b, suggesting two lattice orientations with a ratio of 1.36:1 for interplanar spacing according to the Bragg's law $\lambda = 2nd_{hkl}$, where n is the average index of liquid crystals, d_{hkl} is the interplanar spacing along the [hkl] axis, and h, k, and l are the Miller indices. Kossel diagram analysis further confirms that they are BP $I_{(110)}$ and BP $I_{(200)}$, respectively. This phenomenon severely hinders the accurate construction of the BP mesocrystal. A vertically applied alternative current (AC) electric field (30 V μm^{-1}, 1 kHz) is adopted to supply tilting guidance in addition to the azimuthal guidance caused

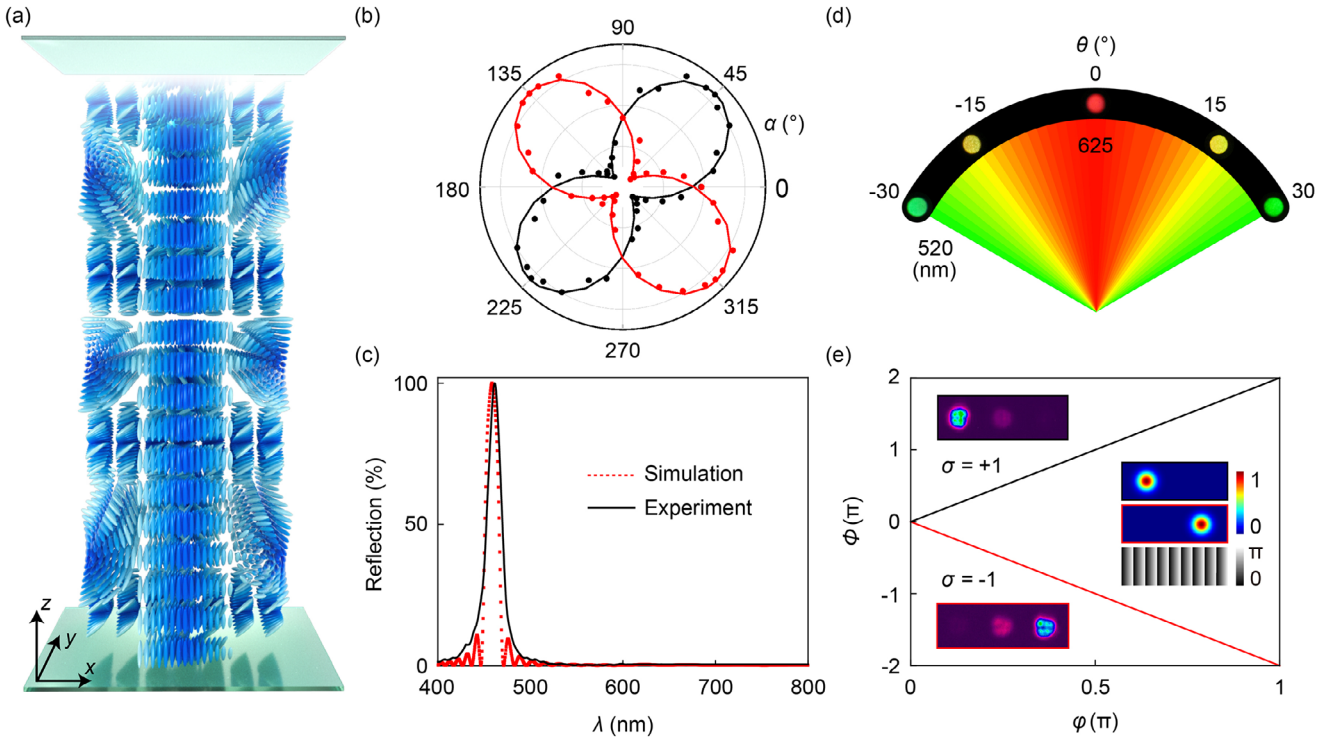

Figure 3. The mapping relationship between the freedom of light and the hierarchy of BPLC mesocrystals. a) Schematic LC director distribution of BP II. b) Dependency of the spin of light σ on the chirality of DTC h. c) Simulated and experimental reflection spectra. d) The dependency of wavelength λ on incident angle θ. e) The dependency of phase Φ on azimuthal orientation of lattice φ. Insets show the simulated and experimental diffraction patterns and preset alignment for BPLC PGs. $\sigma = +1/-1$ indicate LH/RH circular polarization, respectively.

by surface anchoring (Figure S2, Supporting Information). As shown in Figure 2c, the electric field is maintained for 60 s to drive LCs into a homeotropic state through the Fréedericksz transition[12] and heat the system to 31.0 °C by dielectric heating, which is slightly lower than the phase transition point between BP II and BP I (31.3 °C, Figure S3, Supporting Information). After removing the field, the reflectance increases rapidly due to the formation of the BP $I_{(110)}$ monodomain (Figure 2c; Video S1, Supporting Information). Here, the electric field plays two essential roles: First, the electric field drive LCs into a homeotropic state, which serves as an initial uniform phase to avoid martensitic transformation induced polydomain during BP II–BP I phase transition. Second, the dielectric heating to slightly below the phase transition point causes a vertical temperature gradient inside the LC after removing the electric field, leading to the formation of a monodomain BP I with the guidance of the unidirectional alignment. The lattice orientation is the same as the red BP I, suggesting the codirecting effect of both the electric field and surface anchoring works. By this means, a high-quality BP monodomain can be easily generated over the centimeter scale, and vivid colors over the entire visible range can be directly observed with the naked eye (Figure S4, Supporting Information). The chromatic coordinates of the narrow reflection bands are located near the edge in the CIE1931 chromaticity diagram (Figure 2d). They can form a color triangle that is 165% over the standard red, green, and blue (sRGB) space.

2.3. Mapping Relationship Between Optical Freedoms and Hierarchical Structures

The accurate construction of the BP mesocrystals enables the investigation of the structure–activity mechanisms. On the basis of the DTC model of BP II, a theoretical simulation is carried out by the finite difference time domain (FDTD) method (**Figure 3a**; Figure S5, Supporting Information). Since the director cannot be defined in disclinations, an isotropic medium is filled among DTCs (Methods). The black/red lines in Figure 3b exhibit the simulated spin-selective reflectance of the left-handed/right-handed (LH/RH) BP mesocrystals, respectively. The angle α between the transmission axis of the polarizer and the fast axis of the quarter waveplate is tuned to continuously vary the incident polarization. The reflection shows intensive spin selectivity. The calculated maximum/minimum reflectance occurs when the handedness of σ is consistent/inconsistent with that of h, and the experimental results depicted by the black and red dots match well with the simulations. Figure 3c shows the simulated and experimental spin-selective reflection spectra of a BP mesocrystal. They agree with each other, except for a slight deviation of λ due to the minor refractive index mismatching between the ideal and practical BPLCs. Since λ is determined by p, the unique omni-directional spin selectivity of the BP mesocrystal brings a broadband efficient λ filtering effect. Along with varying the incident angle (θ) at the glass substrate/mesocrystal interfaces, different λ values of a white incident beam are selectively reflected

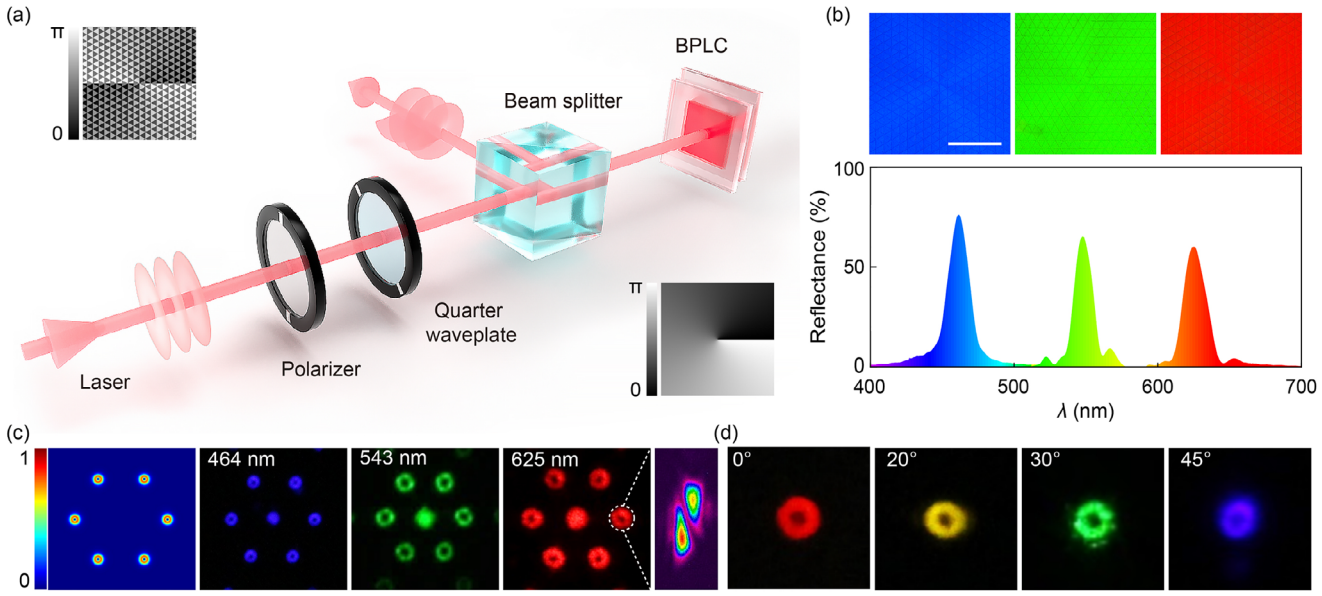

Figure 4. Multi-degree light modulation based on photopatterned BPLC. a) Patterned alignments of a Dammann vortex grating and a *q*-plate and optical setup for characterization. b) POM images and reflection spectra of three Dammann vortex grating-encoded BP mesocrystals. c) Simulated diffraction pattern and experimental results of 464, 543, 625 nm light and topological charge detection. d) θ-dependent wavelength variation of generated optical vortices. The scale bar indicates 200 μm for all POM images.

according to Bragg's law, as presented in Figure 3d. The experimentally recorded reflection spots match well with the simulation. The above simulations and experiments perfectly verify the feasibility of modulating $\{\sigma, \lambda\}$ by manipulating $\{h, p\}$.

The PB phase of reflected light Φ can be independently and precisely preset by spatially tuning the azimuthal orientation of BP lattices φ. In detail, encoded Φ is $\pm$ 2 times φ, while the sign is determined by σ (Figure 3e). In our experiments, we find that the crystallographic direction of $[\bar{1}10]$ maintains a 27° angle with respect to the local alignment direction[21] (Figure S6, Supporting Information), thus enabling precise control over the azimuthal orientation of a BP mesocrystal. For demonstration, we linearly and periodically vary φ in the range of 0–π with a periodicity Λ of 83.3 μm to form a polarization grating (PG), as presented in Figure 3e. Theoretically, orthogonal spins of a 464 nm beam are deflected to $\pm$ 0.33° ($\tan^{-1}(\lambda/\Lambda)$) due to conjugated PB phase modulations of the polarization grating to opposite h. The obtained diffraction angles are ±0.34°, as shown in the insets. Hence, a soft mesocrystal-based platform for multi-degree light modulation is established. The multiple degrees of light $\{\sigma, \lambda, \Phi\}$ can be orthogonally modulated via independently preset freedoms of hierarchical structures $\{h, p, \varphi\}$.

2.4. BP Mesocrystals Enabled Multi-Degree Light Modulations

To validate the efficacy of the platform, a Dammann *q*-plate (DQP) is encoded to the azimuthal orientation of BP mesocrystal. **Figure** 4a depicts the alignment of a DQP with $q = 1/2$ and triple gratings with an including angle of 60° (φ_{DVG}). The POM images presented in Figure 4b verify the feasibility of patterning BP mesocrystals. The grid boundaries caused by azimuth discontinuities match well with the design. Additionally, the sharp reflection spectra suggest perfect uniformity of the lattice orientation inside the mesocrystals regulated by complex anchoring. A reflective optical setup is adopted for the characterization (Figure 4a). σ is set to match the handedness of h by tuning the angle between the linear polarizer and the broadband quarter waveplate. By varying the input λ to match p, hexagonal arrays of optical vortices identical to the simulation are obtained at 464, 543, and 625 nm with high efficiencies (76% for 464 nm, 65% for 543 nm, 60% for 625 nm) (Figure 4c). The optical vortex is featured by a spiral phase of $e^{im\varphi}$, where m and φ are the topological charge and azimuth, respectively. We detect m of the generated optical vortices with the astigmatic transformation method and $m = +1$ as expected.[22] Due to the theoretically infinite number of orthogonal topological states, optical vortices can be used as separate channels for optical information transmission, by which the capacity of the optical network can be drastically enhanced. Here, the 3D DTCs enable omnidirectional σ and λ selective Φ encoding, thus supplying a compact and efficient method for mode processing that is compatible with mature wavelength division multiplexing. A *q*-plate with $q = 1/2$ is further fabricated for the demonstration. Along with increasing θ, only σ with the same handedness as h is reflected and encoded with a spiral phase. Moreover, λ of the generated donut-like optical vortices is gradually blueshifted. Red, yellow, green, and blue optical vortices obtained at different θ are presented in Figure 4d. The results vividly verify the capability of BP mesocrystal in multi-degree light modulation, and the omni-directional σ and λ selective narrow band optical vortex generation is promising in mode/wavelength/spin combined division multiplexing.

Holographic displays are further carried out to demonstrate the superiorities of BP mesocrystals. Notably, a UV polymer stabilization strategy[23] is introduced to stabilize the hierarchical structures, and thereby, the mesocrystals can work at room

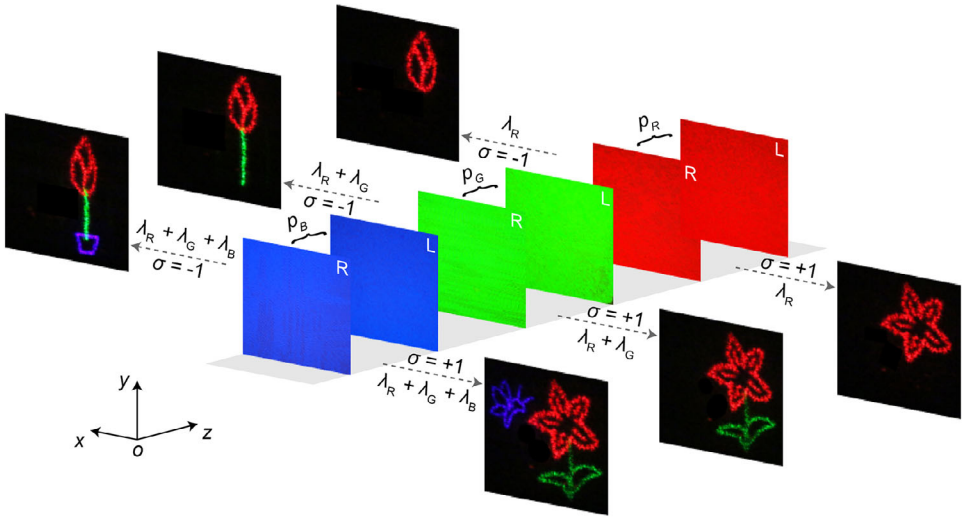

Figure 5. Reconfigurable holographic displays via multi-degree light processing based on BP mesocrystals. L/R indicate LH/RH BP mesocrystals. λ_R = 464 nm, λ_G = 543 nm, and λ_B = 625 nm.

temperature (Figure S7, Supporting Information). The mapping relationship between optical freedoms and hierarchical structures enables a separate spatial phase modulation for various wavelengths with different spins. As shown in **Figure 5**, six holograms are prepared (along the z direction) for three different wavelengths (λ = 464, 543, 625 nm, incident along the z direction) with orthogonal spins. With such stacked layers, different colorful images will be generated for reflected light of different spins. Herein, for easy demonstration, a red bud, a green stem, and a blue pot are generated subsequently for RH circular polarization. A red flower, green stem, and leaves as well as a blue butterfly are observed for LH circular polarization. Both colorful images are decomposed into three monochromatic images and then imprinted into BP layers corresponding to objective chirality and lattice constants (Figure S8, Supporting Information). The designed information is reconstructed free of crosstalk due to the high quality of BP mesocrystals. Herein, the thickness of a single layer is only 8 μm, leading to a low insertion loss. Thanks to the high resolution and rewritability of the photoalignment technique combined with the prime color purity of the BP mesocrystal, more informative chromatic holography can be reasonably expected in a dynamic way.

3. Discussion

BPLC has long been regarded as a 3D photonic crystal due to its omnidirectional periodicity. Here, it is attributed as a soft mesocrystal, thereby high-level orders are considered from a perspective beyond traditional crystallographically. First, chirality is presented as elongated LC molecules assemble to DTCs driven by the strong twisting power of the chiral dopant. Second, the feature size of LC molecules, DTCs, cubic lattices and lateral lattice orientations covers a broad range from single nanometer to microns, thus forming a four-level hierarchy. Finally, since the orientation of cubic lattices is freely programmed, topology can be arbitrarily preset. Large scale uniform monodomains are obtained thanks to the strong surface anchoring suppresses the entropy induced discontinuity in a smooth thermal recycling. Electricity further re-regulates the hierarchal structure across the phase transformation, thus enabling a wide resonance wavelength range covering the whole visible band. The photoalignment enables a convenient patterning of the soft mesocrystal. The one-to-one correspondences between optical freedoms and hierarchical structures makes the multi-degree light modulation totally orthogonal and predictable. Moreover, the external field responsiveness endows the BP mesocrystal with dynamic characteristics. For example, the chirality of DTC can be optically reversed when doped with chiral molecular switches.[24] The lattice constant can be continuously tuned via electrically driven the lattice distortion.[25] The azimuthal orientation of BP lattices can be dynamically reconfigured via photorewriting.[26] Accordingly, the spin, reflective band, and geometric phase of light will be modulated orthogonally according to the structure–activity relationship. It brings deep insights to soft condensed matters,[27] and paves a way for fantastic large-scale parallel and multi-degree light modulations promising in optics and photonics.[28]

4. Conclusion

In summary, a multi-degree light modulation is realized based on the hierarchical architecture of a soft mesocrystal. Large-area uniform BP mesocrystals are obtained via precisely architecting the hierarchical structure with the assistance of photoalignment anchoring and electricity. The mapping relationship between the chirality of the DTC, lattice constant, azimuthal orientation of lattices and the spin, wavelength, geometric phase of light is established. It enables a predictable way to orthogonally modulate the multiple degrees of light. Omnidirectional spin/wavelength selective OAM generation and multichannel color holographic display are presented for proof demonstration. This work explores the potential of mesocrystals in multi-degree light modulation, and may upgrade existing optical computing, optical communications, and holographic displays.

5. Experimental Section

Materials: The BPLC was mixed with a host nematic LC HTW114200-050 ($\Delta\epsilon \approx 10.9$ at 1 kHz, 20 °C; $\Delta n \approx 0.222$ and $n_e \approx 1.729$ at 589 nm, 20 °C; HCCH, China), chiral dopant S811 or R811 (HTP = 8.3 μm^{-1} at 30 °C, NCLCP, China), reactive mesogen RM257 (NCLCP, China), 2-ethylhexyl acrylate (EHA, Sigma–Aldrich, USA), and photoinitiator Omnirad 651 (BASF, Germany) with weight ratios of 91.5:4.0:4.0:0.5. The ratio of chiral dopant was adjusted to tune *p*. After stirring, all precursor was capillary infiltrated into an 8 µm-thick photoalignment cell above the clearing point, and then the temperature decreases at a rate of −0.3°C min^{-1} with an LTS 120 hot stage (Linkam, UK). Polymer stabilization was carried out by illumination under a 365 nm LED (Thorlabs, USA) for 90 min at ≈200 µW cm^{-2}. To enhance the structural robustness, samples are UV polymerized under temperatures of 37.0, 31.0, and 32.0 °C for red, green, and blue BPs, respectively. The temperatures are optimized for sharp and high reflection spectra.

Cell Fabrication: After ultrasonic bath and UV–ozone cleaning, the indium–tin-oxide glass-coated substrates were spin-coated with photoalignment agent SD1 (NCLCP, China) dissolved in dimethylformamide (DMF, Sigma–Aldrich, USA) at a concentration of 0.3 wt.% and then baked at 100 °C for 10 min. Two pieces of substrates were sealed with epoxy glue mixed with 8-µm spacers to form a cell. The photoalignment is performed with a 1920 × 1080 pixelated digital micromirror device-based microlithography system (NCLCP, China).

Simulations: Based on the DTC model, the unit cell is divided into 37 × 37 × 37 grids. The dielectric tensor distribution is calculated using a uniaxial anisotropic medium with ordinary refractive index $n_o = 1.55$ and extraordinary refractive index $n_e = 1.64$. The space among DTCs is assumed to be filled with an isotropic medium with an average refractive index $n = (2n_o + n_e)/3$. The lattice constants $p = 144$ nm and $p = 200$ nm are used for normal and tilted incidences, respectively. The lateral boundary condition is fixed as a periodical boundary condition. The boundaries in and normal to the light propagation direction are set as the perfect matching layer and periodical (normal incidence)/ Bloch boundary condition (tilted incidence), respectively. All the simulations are carried out with the commercial software Lumerical FDTD Solutions.

Characterizations: The transmission spectra were recorded with a spectrometer (PG2000-pro, Ideaoptics, China). All the reflection spectra are measured with an incidence of matched circular polarization. All micrographs were captured under the reflective mode of a polarization optical microscope (Nikon 50i, Japan), and the Kossel diffraction was operated under a microscope (Olympus, BX51, Japan). Monochromatic and white beams are output by a supercontinuum laser (SuperK EVO, NKT Photonics, Denmark) and a multichannel acousto-optic tunable filter (SuperK SELECT, NKT Photonics, Denmark). Diffraction patterns are captured by a digital camera (EOS M, Canon, Japan). A 1 kHz AC square-wave electric signal is generated by a function generator (33522B, Agilent, USA) and amplified by a voltage amplifier (2340, TEGAM, USA).

Supporting Information

Supporting Information is available from the Wiley Online Library or from the author.

Acknowledgements

The authors gratefully acknowledge the support of the National Key Research and Development Program of China (2022YFA1203703), the National Natural Science Foundation of China (NSFC) (62035008), the Natural Science Foundation of Jiangsu Province (BK20212004) and the Fundamental Research Funds for the Central Universities (021314380233). The authors appreciate Qinyu Mo and Jinbing Wu for their constructive discussions.

Conflict of Interest

The authors declare no conflict of interest.

Data Availability Statement

The data that support the findings of this study are available from the corresponding author upon reasonable request.

Keywords

blue phase liquid crystals, hierarchical architectures, light–matter interaction, mesocrystals, multi-degree light modulations

Received: December 5, 2023
Revised: January 15, 2024
Published online: February 6, 2024

[1] H. Cölfen, M. Antonietti, *Angew. Chem., Int. Ed.* **2005**, *44*, 5576.
[2] M. Niederberger, H. Cölfen, *Phys. Chem. Chem. Phys.* **2006**, *8*, 3271.
[3] J. Seto, Y. Ma, S. A. Davis, F. Meldrum, A. Gourrier, Y. Y. Kim, U. Schilde, M. Sztucki, M. Burghammer, S. Maltsev, C. Jäger, H. Cölfen, *Proc. Natl. Acad. Sci. U.S.A.* **2012**, *109*, 3699.
[4] X. Qiu, X. Wang, Y. He, J. Liang, K. Liang, B. L. Tardy, J. J. Richardson, M. Hu, H. Wu, Y. Zhang, O. J. Rojas, I. Manners, J. Guo, *Sci. Adv.* **2021**, *7*, eabh3482.
[5] Z. Zhang, T. Tsuchimochi, T. Ina, Y. Kumabe, S. Muto, K. Ohara, H. Yamada, S. L. Ten-no, T. Tachikawa, *Nat. Commun.* **2022**, *13*, 1499.
[6] X. L. Wu, S. J. Xiong, Z. Liu, J. Chen, J. C. Shen, T. H. Li, P. H. Wu, P. K. Chu, *Nat. Nanotechnol.* **2011**, *6*, 103.
[7] a) S. Mann, *Nat. Mater.* **2009**, *8*, 781; b) L. Zhou, P. O'Brien, *J. Phys. Chem. Lett.* **2012**, *3*, 620; c) G. Zhu, M. L. Sushko, J. S. Loring, B. A. Legg, M. Song, J. A. Soltis, X. Huang, K. M. Rosso, J. J. De Yoreo, *Nature* **2021**, *590*, 416.
[8] a) N. Yu, P. Genevet, M. A. Kats, F. Aieta, J.-P. Tetienne, F. Capasso, Z. Gaburro, *Science* **2011**, *334*, 333; b) S. Sun, Q. He, S. Xiao, Q. Xu, X. Li, L. Zhou, *Nat. Mater.* **2012**, *11*, 426.
[9] D.-K. Yang, S.-T. Wu, *Fundamentals of Liquid Crystal Devices*, John Wiley & Sons, Hoboken, New Jersey, **2014**.
[10] a) P.-G. De Gennes, J. Prost, *The Physics of Liquid Crystals*, Oxford University Press, New York, **1993**. b) W. Park, J. Lee, M. J. Han, J. Wolska, D. Pociecha, E. Gorecka, M.-K. Seo, Y.-S. Choi, D. K. Yoon, *ACS Appl. Mater. Interfaces* **2022**, *14*, 4409.
[11] D. C. Wright, N. D. Mermin, *Rev. Mod. Phys.* **1989**, *61*, 385.
[12] J. Yang, W. Zhao, W. He, Z. Yang, D. Wang, H. Cao, *J. Mater. Chem. C* **2019**, *7*, 13352.
[13] a) E. Otón, P. Morawiak, K. Gaładyk, J. M. Otón, W. Piecek, *Opt. Express* **2020**, *28*, 18202; b) Z. G. Zheng, C. L. Yuan, W. Hu, H. K. Bisoyi, M. J. Tang, Z. Liu, P. Z. Sun, W. Q. Yang, X. Q. Wang, D. Shen, *Adv. Mater.* **2017**, *29*, 1703165; c) J. Yan, S. T. Wu, K. L. Cheng, J. W. Shiu, *Appl. Phys. Lett.* **2013**, *102*, 081102.
[14] a) J. A. Martínez-González, X. Li, M. Sadati, Y. Zhou, R. Zhang, P. F. Nealey, J. J. de Pablo, *Nat. Commun.* **2017**, *8*, 15854; b) S. Liu, I. Nys, K. Neyts, *Adv. Opt. Mater.* **2022**, *10*, 2200711; c) X. Xu, J. Wang, Y. Liu, D. Luo, *Adv. Photonics Nexus* **2023**, *2*, 026004.
[15] H. Claus, O. Willekens, O. Chojnowska, R. Dąbrowski, J. Beeckman, K. Neyts, *Liqid Crystals* **2016**, *43*, 688.
[16] R. Suryantari, Y.-H. Shih, Y.-H. Shih, H.-Y. Chen, C.-S. Wu, C.-Y. Huang, *Opt. Lett.* **2023**, *48*, 77.
[17] C. W. Chen, C. T. Hou, C. C. Li, H. C. Jau, C. T. Wang, C. L. Hong, D. Y. Guo, C. Y. Wang, S. P. Chiang, T. J. Bunning, I. C. Khoo, T. H. Lin, *Nat. Commun.* **2017**, *8*, 727.

[18] S. Cho, M. Takahashi, J.-I. Fukuda, H. Yoshida, M. Ozaki, *Commun. Mater.* **2021**, *2*, 39.
[19] a) E. Cohen, H. Larocque, F. Bouchard, F. Nejadsattari, Y. Gefen, E. Karimi, *Nat. Rev. Phys.* **2019**, *1*, 437; b) P. Chen, B. Y. Wei, W. Hu, Y. Q. Lu, *Adv. Mater.* **2020**, *32*, 1903665.
[20] X. Li, J. A. Martínez-González, O. Guzmán, X. Ma, K. Park, C. Zhou, Y. Kambe, H. M. Jin, J. A. Dolan, P. F. Nealey, J. J. D. Pablo, *Sci. Adv.* **2019**, *5*, eaax9112.
[21] J.-I. Fukuda, S. Žumer, *Phys. Rev. Res.* **2020**, *2*, 033407.
[22] P. Chen, L. L. Ma, W. Duan, J. Chen, S. J. Ge, Z. H. Zhu, M. J. Tang, R. Xu, W. Gao, T. Li, *Adv. Mater.* **2018**, *30*, 1705865.
[23] H. Kikuchi, M. Yokota, Y. Hisakado, H. Yang, T. Kajiyama, *Nat. Mater.* **2002**, *1*, 64.
[24] P. Chen, L.-L. Ma, W. Hu, Z.-X. Shen, H. K. Bisoyi, S.-B. Wu, S.-J. Ge, Q. Li, Y.-Q. Lu, *Nat. Commun.* **2019**, *10*, 2518.
[25] a) M. Wang, C. Zou, J. Sun, L. Zhang, L. Wang, J. Xiao, F. Li, P. Song, H. Yang, *Adv. Funct. Mater.* **2017**, *27*, 1702261; b) D.-Y. Guo, C.-W. Chen, C.-C. Li, H.-C. Jau, K.-H. Lin, T.-M. Feng, C.-T. Wang, T. J. Bunning, I. C. Khoo, T.-H. Lin, *Nat. Mater.* **2020**, *19*, 94.
[26] V. G. Chigrinov, V. M. Kozenkov, H.-S. Kwok, *Photoalignment of Liquid Crystalline Materials: Physics and Applications*, John Wiley & Sons, Hoboken, New Jersey, **2008**.
[27] a) K. R. Schlafmann, T. J. White, *Nat. Commun.* **2021**, *12*, 4916; b) A. Nych, J.-I. Fukuda, U. Ognysta, S. Žumer, I. Muševič, *Nat. Phys.* **2017**, *13*, 1215.
[28] a) F. Meng, C. Zheng, W. Yang, B. Guan, J. Wang, T. Ikeda, L. Jiang, *Adv. Funct. Mater.* **2022**, *32*, 2110985; b) F. Castles, F. V. Day, S. M. Morris, D. H. Ko, D. J. Gardiner, M. M. Qasim, S. Nosheen, P. J. W. Hands, S. S. Choi, R. H. Friend, H. J. Coles, *Nat. Mater.* **2012**, *11*, 599; c) W. Cao, A. Muñoz, P. Palffy-Muhoray, B. Taheri, *Nat. Mater.* **2002**, *1*, 111.